KeAi
CHINESE ROOTS
GLOBAL IMPACT

Contents lists available at ScienceDirect

Petroleum Science





Original Paper

Surface erosion thickness and oxygen isotope of the Early Jurassic lake water in northern Sichuan Basin, evidence from clumped isotopes of shell limestones



Ping-Ping Li ^{a,b,c,*}, Shi-Jie He ^b, Zhan-Jie Xu ^b, Dai-Qin Jiang ^b, Hua-Yao Zou ^{a,b}, Fang Hao ^d

- ^a State Key Laboratory of Petroleum Resources and Engineering, China University of Petroleum (Beijing), Beijing, 102249, China
- ^b College of Geosciences, China University of Petroleum (Beijing), Beijing, 102249, China
- ^c Carbonate Research Center, China University of Petroleum (Beijing), Beijing, 102249, China
- ^d State Key Laboratory of Deep Oil and Gas, China University of Petroleum (East China), Qingdao, 266580, Shandong, China

ARTICLE INFO

Article history: Received 9 July 2024 Received in revised form 30 March 2025 Accepted 29 May 2025 Available online 1 June 2025

Edited by Xi Zhang and Jie Hao

Keywords: Surface erosion thickness δ¹⁸O of Jurassic lake water Clumped isotopes Shell limestone Sichuan Basin

ABSTRACT

Oxygen isotope (δ^{18} O) of paleolake water is a key indicator for reconstructing the formation temperature and diagenetic history of lacustrine carbonate minerals. In this study, we use clumped isotopes (Δ_{47}) of lacustrine shell limestones to determine the surface erosion thickness and $\delta^{18}O$ of Early Jurassic lake water in the northern Sichuan Basin. We analyzed nine shell limestone and seventeen shale samples from the Early Jurassic Da'anzhai Member (J_1z^4) in the Yuanba area. Whether the shell's shapes are well or partially preserved, the I_1z^4 shell limestones in the Yuanba area show no significant recrystallization and dull cathodoluminescence. These characteristics suggest that the shell limestones did not undergo significant diagenetic alteration during late burial. The Δ_{47} values of the $I_1 Z^4$ shell limestones range from $0.448 \pm 0.005\%$ to $0.463 \pm 0.006\%$, yielding clumped isotope temperature ($T_{\Delta 47}$) of 64.4 \pm 0.8 to 69.7 \pm 1.4 °C, which is significantly higher than the Early Jurassic paleotemperature. It suggests that the Δ_{47} of shell limestones was altered by solid-state reordering, meaning the $T_{\Lambda47}$ does not reflect the initial formation temperatures. By integrating organic matter's maturation model (Easy% R_0) of coexisting shales with Δ_{47} solid-state reordering model of calcite, we constrained the maximum burial temperature (~170 °C) and the initial formation temperature (~28 °C) of these shell limestones. Based on reported paleotemperature gradient, we estimated that the surface erosion thickness was about 1500 m. Furthermore, using the determined initial formation temperatures and conventional oxygen isotope thermometer, we determined that the δ^{18} O values of the Early Jurassic lake water in the Sichuan Basin, which ranged from -10.8% to -8.0% (SMOW). The reconstructed paleotemperature and δ^{18} O of lake water suggest that the Early Jurassic in the Sichuan Basin was warm and humid, which was favorable for the deposition of organic-rich lacustrine shale. The methods developed in this study, which employ Δ_{47} of shell limestones to reconstruct the maximum burial temperature and paleolake environmental conditions, demonstrate broad applicability to the Sichuan Basin and similar lacustrine basins.

© 2025 The Authors. Publishing services by Elsevier B.V. on behalf of KeAi Communications Co. Ltd. This is an open access article under the CC BY license (http://creativecommons.org/licenses/by/4.0/).

1. Introduction

Oxygen isotope $(\delta^{18}O)$ values of diagenetic fluids, such as sea and lake water, are crucial for determining the formation

E-mail address: lpp@cup.edu.cn (P.-P. Li).

Peer review under the responsibility of China University of Petroleum (Beijing).

temperature of carbonate minerals that deposited in these fluids using conventional oxygen isotope thermometers (Kim and O'Neil, 1997; Horita, 2014; Guo et al., 2021). The δ^{18} O evolution curve of Phanerozoic seawater has been widely studied (Veizer et al., 1997, 1999; Veizer and Prokoph, 2015). However, no uniform δ^{18} O evolution of lake water has been recorded, because the lake water in certain geological time can be completely different due to the difference in balance between the freshwater input and evaporation (Hladyniuk and Longstaffe, 2016; Haig et al., 2021; Holmes et al., 2023; Wang et al., 2023a).

^{*} Corresponding author.

 δ^{18} O reconstruction in sea or lake water is mainly based on the δ¹⁸O fractionation between authigenic materials and fluids (Veizer et al., 1997, 1999; Wallmann, 2001; Veizer and Prokoph, 2015). The authigenic materials mainly include skeletal calcite (e.g. brachiopods, foraminifera, belemnites), skeletal apatite, chert, dolomite and calcite in forms of cements and bulk rock samples (Jaffrés et al., 2007; Veizer and Prokoph, 2015). According to the conventional oxygen isotope thermometers, determination of the δ^{18} O values of diagenetic fluids requires the knowledge of both the δ^{18} O values and formation temperatures of authigenic materials (Kim and O'Neil, 1997). The δ^{18} O values of authigenic materials can be easily measured, but these values can be altered by diagenetic alterations. As a result, only unaltered samples can be used to determine $\delta^{18}O$ values of diagenetic fluids. A more fundamental challenge lies in determining the initial formation temperatures of these materials, which are typically unknown and difficult to constrain (Eiler, 2007). In current studies, the initial formation temperatures of authigenic materials are usually determined from empirical statistical fitting (Veizer and Prokoph, 2015), which makes it difficult to accurately reconstruct the sea or lake water δ^{18} O.

The carbonate clumped isotope thermometer (Δ_{47} , the abundance of mass-47 CO₂) provides a powerful tool for directly determining the formation temperature of carbonate minerals without known of the δ^{18} O of diagenetic fluids (Ghosh et al., 2006; Eiler, 2007). Instead, the δ^{18} O of diagenetic fluid, from which carbonate minerals were deposited, can be directly determined using the δ^{18} O of carbonate minerals and formation temperature, based on conventional oxygen isotope thermometer (Ferry et al., 2011; Li et al., 2020). This approach has significantly improved our ability to reconstruct the δ^{18} O of diagenetic fluid (Cummins et al., 2014; Henkes et al., 2018; Banerjee et al., 2023). However, carbonate minerals usually experienced post-depositional diagenetic alteration during burial under elevated temperatures (Wu and Wu, 1996; Winkelstern and Lohmann, 2016; Wang et al., 2023b). Consequently, the clumped isotope temperature of carbonate minerals $(T_{\Delta 47})$ cannot represent the initial formation temperature (Passey and Henkes, 2012; Henkes et al., 2014). The $T_{\Delta 47}$ is mainly affected by two primary mechanisms: diagenetic alteration (recrystallization) and solid-state reordering (C-O bond exchange in solid minerals) (Henkes et al., 2014; Ryb and Eiler, 2018). In cases where carbonate minerals experienced diagenetic alteration (recrystallization at higher temperature), the $T_{\Delta 47}$ will represent the final balanced temperature instead of the initial formation temperature. For carbonate minerals didn't experience diagenetic alterations, the $T_{\Delta47}$ would be only affected by solid-state reordering, which can be constrained by kinetic models depending on a given thermal history (Henkes et al., 2014; Stolper and Eiler, 2015; Lloyd et al., 2018; Hemingway and Henkes, 2021). Taking calcite for example, $T_{\Delta 47}$ will: 1) not change when the burial temperature is lower than 100 °C; 2) increase gradually (resulting from solid-state reordering) when the burial temperature exceeds 100 °C; 3) reach the surrounding temperature when the burial temperature exceeds about 200 °C; 4) decrease if the burial temperature decreases below 200 °C during subsequent uplift (Stolper and Eiler, 2015). Theoretically, if the $T_{\Delta 47}$ of carbonate minerals was only related to solid-state reordering, the experienced thermal history (such as the maximum burial temperature) can be constrained by the solid-state reordering model using the initial formation age, temperature and measured $T_{\Delta 47}$ (Li et al., 2020, 2021; Ryb et al., 2021).

The Early Jurassic Da'anzhai Member (J₁z⁴), deposited during the global Toarcian oceanic anoxic event (T-OAE), consists predominantly of lacustrine shales and shell limestones (Xu et al., 2017a, 2020). The carbon sequestration and organic matter enrichment in the Sichuan Basin was discussed during the global

oceanic anoxic event (Xu et al., 2017a), but the paleotemperature and $\delta^{18}O$ of the Early Jurassic lake water in the Sichuan Basin were not explored, which restricted the understanding on the organic matter formation and preservation in this era. In addition, the formation temperatures and precipitation stages of the calcite veins in the Jurassic shales were difficult to constrain due to the unknown $\delta^{18}O$ value of the Jurassic lake water when applying conventional oxygen isotope thermometers. The present burial temperature of the J_1z^4 is close to 100 °C, which means that the maximum burial temperature of the J_1z^4 exceeds 100 °C because multiple uplifts and exhumations events occurred since the Late Cretaceous in the Sichuan Basin (Liu et al., 2021). This suggest that shell limestones experienced solid-state reordering, which can be used to constrain the maximum burial temperature and surface erosion thickness in the Sichuan Basin.

The purpose of this paper is to determine the maximum burial temperature and surface erosion thickness, paleotemperature and δ^{18} O of the Early Jurassic lake water in the northern Sichuan Basin, using clumped isotope of unaltered shell limestones. The results will supply new constrains on the burial, exhumation histories and paleoenvironments of the Early Jurassic lake in the northern Sichuan Basin.

2. Geologic setting

The Sichuan Basin, locating in southwestern China, was formed on top of the Pre-Sinian basement and consists of thick marine and continental sediments, which were deposited during six tectonic orogenies: the Yangtze (before 630 Ma), Caledonian (630–320 Ma), Hercynian (320–252 Ma), Indosinian (252–195 Ma), Yanshanian (195–65 Ma), and Himalayan (65–0 Ma) (Zhai, 1989). The Sichuan Basin was mainly developed in relatively extensional settings before the Indosinian with the deposition of marine carbonates and shales, while it was mainly developed in relatively compressional settings since the Late Indosinian with the deposition pf continental sandstones and shales (Zhai, 1989; Ma et al., 2008; Liu et al., 2021).

At the end of the Late Triassic, the Sichuan Basin was covered by the Upper Triassic Xujiahe Formation (T₃x) consisting of continental sandstones and shales, which were developed in a deltalacustrine environment (Zhu et al., 2009). Subsequently, the Sichuan Basin was covered by the Lower Jurassic Ziliujing Formation (J₁z) consisting of shales and shell limestones, which were mainly developed in a lacustrine environment (Wang et al., 2020). The J_1z can be divided into four members from bottom to the top: Zhenzhuchong (J_1z^1) , Dongyuemiao (J_1z^2) , Ma'anshan (J_1z^3) and Da'anzhai (J_1z^4) . Among which, the J_1z^4 can be divided into three sub-members from bottom to top: the third sub-member consists of thin shell limestones and shales, the second sub-member consists of thick shales and thin shell limestones, and the first submember consists of thin shales and thick shell limestones (Jiang et al., 2023). After deposition of the J₁z, the Sichuan Basin was covered by the Middle and Upper Jurassic sandstones and shales which were mainly deposited in lacustrine to fluvial environments.

At the end of the Late Jurassic, limited uplift and denudation of Upper Jurassic units occurred in the Sichuan Basin (Liu et al., 2021). Then, the Sichuan Basin was covered by thick Cretaceous sandstones, conglomerates, and red shales. High uplift and denudation occurred since the Late Cretaceous resulting in the preservation of thin Cretaceous covers at the surface of the northern Sichuan Basin (Li et al., 2016). In the central part of the Sichuan Basin, Cretaceous covers were completely eroded leading to the surface exposure of Upper Jurassic sediments (Li et al., 2016).

According to previous studies using apatite fission track data, the uplift and denudation since the Late Cretaceous can be roughly

divided into three stages: high uplift and denudation during 120–80 Ma, low uplift and denudation during 80–30 Ma, and high uplift and denudation since 30 Ma caused by the Himalaya movement (Deng et al., 2013).

The Yuanba area is situated in the northern Sichuan Basin, adjacent to the southern margin of the Micang Uplift. This region comprises several secondary structural units: Cangxi-Bazhong gentle slope, Jiulongshan anticline, Chixi depression, Tongnanba anticline and Tongjiang depression (Li et al., 2015). The sampling wells (YY2 and YB273) in this study are located in the Cangxi-Bazhong gentle slope characterized by weak structural deformations (Fig. 1).

3. Samples and analytical methods

Nine J_1z^4 shell limestone samples (seven samples from the well YY2, and two samples from the well YB273), and seventeen J_1z^4 shale samples from the well YY2 were collected from the Yuanba area, northern Sichuan Basin. Typical pictures of bulk shell limestone samples are shown in the Supplemental data Fig. 1. Shell limestone samples were analyzed for petrology and geochemistry, and shale samples were analyzed for vitrinite reflectance (R_0).

Petrology, XRD (X-ray diffraction) and R_0 were analyzed at the National Key Laboratory of Petroleum Resources and Engineering, China University of Petroleum (Beijing). All bulk rock samples of shell limestones were used to make thin sections for Petrology and cathodoluminescence (CL) observations. The thin sections were made using standard methods, with polished on one side and thickness about 0.04 mm. Petrology observations of the shell limestone samples were analyzed under transmitted light and cathodoluminescent light using a microscope (Nikon LV100N POL)

and a cathodoluminometer (BII CLF-2) with an operating current of 330 μ A and a beam voltage of 10 kV. Bulk rock samples were ground to powder less than 100 mesh using an agate mortar at room temperature. Then, the powders were used to run XRD analyses using a BRUKER D2 PHASER with an operating current of 10 mA and voltage of 30 kV. Organic petrography and R_0 were analyzed by a Leica DM4500P microscope equipped with CRAIC microscope photometer using conventional microphotometric methods. After the microscope was calibrated using standards, R_0 values were collected by the Hilgers Technisches Büero Fossil system. Each sample was analyzed for 20–30 measurement points of vitrinite and 1σ standard deviation was generally below 0.1%.

The δ^{13} C, δ^{18} O, and clumped isotope (Δ_{47}) of shell limestone samples were analyzed at the Institute of Geology and Geophysics, Chinese Academy of Sciences. Firstly, all the powders from bulk shell limestone samples were extracted with dichloromethane (DCM) for 24 h at room temperature to remove soluble organic matter as a little condensed oil produced during the J_1z^4 shale gas testing. Secondly, the powders were reacted with 3% H₂O₂ for 4 h to remove residual organic matters, following the procedures described by Eagle et al. (2010). Finally, about 10 mg of carbonate powders for each sample were reacted with 103% phosphoric acid at 90 °C. The CO₂ produced during the reaction was purified and measured using a Thermo MAT253 gas-source isotope ratio mass spectrometer, following the procedures introduced by Ghosh et al. (2006) and Wang et al. (2016a). The mass 44-49 CO₂ for each sample and reference gas (high-purity CO₂) was measured in nine acquisitions, then Δ_{47} was calculated using the following equation.

$$\Delta_{47} = \left[\left(\frac{R_{47}}{R_{47^*}} \right) - \left(\frac{R_{46}}{R_{46^*}} \right) - \left(\frac{R_{45}}{R_{45^*}} \right) \right] \times 1000 \tag{1}$$

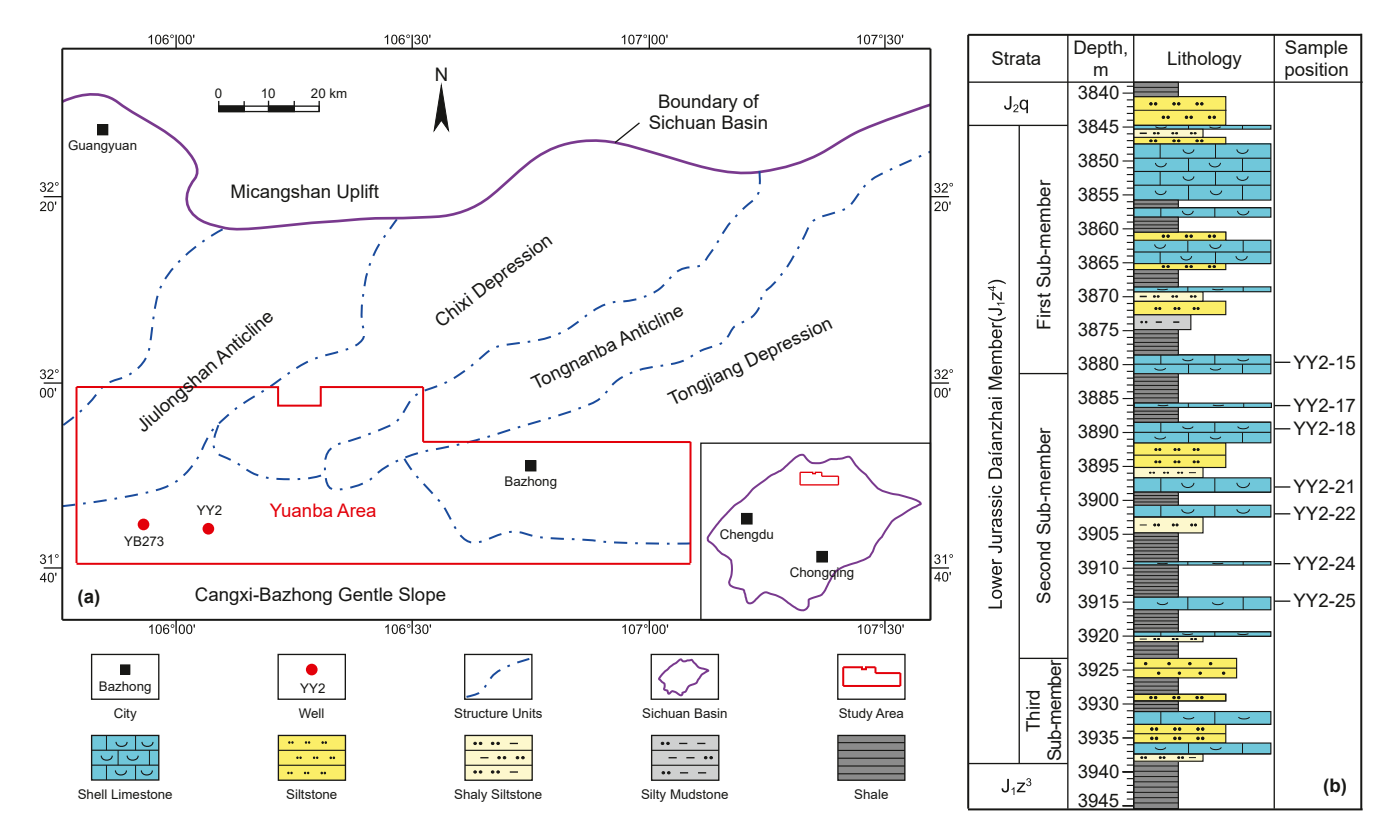


Fig. 1. Location of wells in the Yuanba area in the northeastern Sichuan Basin (a), and stratigraphic sequence of the Lower Jurassic Da'anzhai Member (J_1z^4) of the well YY2 (b). $J_2q = Middle$ Jurassic Qianfuya Formation, $J_1z^3 = Lower$ Jurassic Ma'anshan Member.

where the R_{45} , R_{46} , R_{47} represent the measured abundance ratios of mass 45, 46, and 47 relatives to mass 44, respectively, while R_{45^*} , R_{46^*} , R_{47^*} denote the corresponding ratios under conditions of stochastic isotope distribution.

Each sample was measured in triplicate, with the error calculated by standard deviation divided by $\sqrt{3}$. The δ^{13} C, δ^{18} O, and raw Δ_{47} values of shell limestone samples were calculated following the method provided by Huntington et al. (2009). Thirdly, the raw Δ_{47} values were converted into the absolute reference frame (Δ_{47} , CDES 90 °C) using the solid carbonate standards (ETH1~ETH4) and the InerCarb (NB4 and P1) method (Bernasconi et al., 2018). The raw data of d45–d49 of samples and standards was listed in the Supplementary data. Finally, the clumped isotope temperatures ($T_{\Delta47}$) were calculated using the following calibration equation built by Dennis et al. (2011) as $T_{\Delta47}$ of the shell limestone samples were quite similar to the temperature ranges suitable for Dennis' equation.

$$\Delta_{47} = \frac{0.0636 \times 10^6}{T^2} - 0.0047 \tag{2}$$

The detailed data of δ^{13} C, δ^{18} O, and raw Δ_{47} values were listed in the Supplementary data. The δ^{18} O of lake water was calculated using the equation proposed by Kim and O'Neil (1997) basing on the initial formation temperature (see in the discussion) and δ^{18} O of shell limestone samples. The solid-state reordering model used in this study was the exchange-diffusion model (Stolper and Eiler, 2015). For a given initial formation temperature and time-temperature history, the Δ_{47} or $T_{\Delta47}$ evolution of carbonate materials can be modeled using the exchange-diffusion model. A free software package for running the reordering models was introduced by Lloyd et al. (2018).

4. Results

4.1. Petrography and X-ray diffraction

Petrography observations of thin-sections under plane polarized light reveals that the shell limestones from the Yuanba area are mainly consist of bioclastic shells, with minor quartz and dark organic materials dispersed throughout the matrix. The bioclastic shells, consisting mainly of bivalves, ostracods and gastropods, are in close linear contact with each other (Fig. 2). According to the morphology of bioclastic shells, the shell limestone in the Yuanba area can be classified into two distinct types: (1) well-preserved shells (SWP; Fig. 2(a)-(c), (g)) that maintain their original morphology and are readily identifiable in thin section, and (2) partially preserved shells (SPP; Fig. 2(h)-(i)) that occur as fragmented bioclasts with incomplete morphological features. Only a few shells in Fig. 2(a) show local cleavage cracks, but most other shells or shells' fragments didn't show such cleavage cracks. Under cathodoluminescence light, both SWP and SPP shell types appear dark and with no cathodoluminescence (Fig. 2(d)-(f), (j)). Only shell limestones from samples YY2-25 and YB273-7 have weak cathodoluminescence (Fig. 2(k)-(1)). However, the dark organic matters between the shells has bright yellow or blue cathodoluminescences (Fig. 2(d)–(f), (j)–(1)), which is consistent with the fact that the coexisting shales produced a small amount of condensate oil (Xu et al., 2020).

The X-ray diffraction (XRD) results of the shell limestone samples after DCM extraction and H_2O_2 treatment are shown in Table 1. The main mineral composition of the shell limestones is calcite (typically 82.7%–97.6%), with minor quartz (2.4%–23.7%), hematite, and clay (typically less than 5%).

4.2. Vitrinite reflectance (R_0)

According to the microscopic observation, the organic constituents of the I₁z⁴ shale in the Yuanba area are sapropelinite, exinite, vitrinite, intertinite and amorphous solid bitumen (Fig. 3). Due to relatively high organic maturity (R_0 >1.2%, Table 2), it is difficult to distinguish the sapropelinite and exinite under the microscope. The vitrinite consists of structural vitrinite, non-structure vitrinite. and fragmentary vitrinite, and is dark grey to grey under the oilimmersed reflectance light with non-fluorescence (Fig. 3(a)-(d)). The intertinite is usually light grey to white under the oilimmersion reflected light with non-fluorescence (Fig. 3(e)). The amorphous solid bitumen belongs to the secondary organic matter transformed by hydrocarbon generations process, and is light grey under the oil-immersed reflectance light and mainly distributed in the space between the inorganic minerals (Fig. 3(f)). The R_0 values of the 17 J_1z^4 shale samples are mainly in the range of 1.28%–1.47% (average of 1.36%, Fig. 4), which indicate that the organic constituents of the J₁z⁴ shale reached high to over maturity stage. This is consistent with the production of minor condensate oil by the J_1z^4 shale in the Yuanba area.

4.3. δ^{13} C, δ^{18} O, Δ_{47} , and clumped isotope temperature $(T_{\Delta47})$

Detailed values of δ^{13} C, δ^{18} O, and Δ_{47} of the J_1z^4 shell limestones in the Yuanba area are shown in Table 3. The δ^{13} C and δ^{18} O values of the shell limestones range from 3.163 \pm 0.005‰ to 4.159 \pm 0.009‰, and $-14.820 \pm$ 0.009‰ to $-10.231 \pm$ 0.006‰, respectively. The Δ_{47} (CDES90) values corrected by the ETH standard range from 0.448 \pm 0.005‰ to 0.463 \pm 0.006‰, and the clumped isotope temperatures ($T_{\Delta 47}$) range from 64.4 \pm 0.8 to 69.7 \pm 1.4 °C (average of 67.2 \pm 1.4 °C, Fig. 5), according to the temperature calibration equation established by Dennis et al. (2011). There is no significant difference in δ^{13} C, δ^{18} O and $T_{\Delta 47}$ of the SWP and SPP shell limestones, and shell limestones with weak or no cathodoluminescence.

5. Discussion

5.1. Maximum burial temperature and erosion thickness during late uplift

For sedimentary basins experienced early subsidence and late large-scale uplift and denudation, the amount of surface erosion is important to reconstruct the basin evolution history as well as the maturation of the underlying source rocks (English et al., 2016). Multiple uplifts and denudations occurred since 100 Ma in the Sichuan Basin (Deng et al., 2013), resulting in limited Cretaceous or Upper Jurassic directly exposed at the surface (Li et al., 2016). Consequently, it is difficult to reconstruct the detailed basin evolution of the Sichuan Basin. Therefore, the erosion thickness during the late uplift event has become a key parameter governing the burial and thermal evolution of the Sichuan Basin.

Conventional methods for restoration of erosion thickness include the acoustic log method, R_0 vs. depth, and thickness correlation with un-eroded strata (Magara, 1976; Dow, 1977; Heasler and Kharitonova, 1996). However, large-scale lateral compression since the Late Cretaceous (Deng et al., 2013; Liu et al., 2021) has resulted in the compaction of shallow burial strata, which was completely different from the normal mechanical compaction in the Sichuan Basin. As a result, the acoustic log method is not suitable for determining surface erosion thickness in the Sichuan Basin. In addition, regional uplift and denudation since the Late

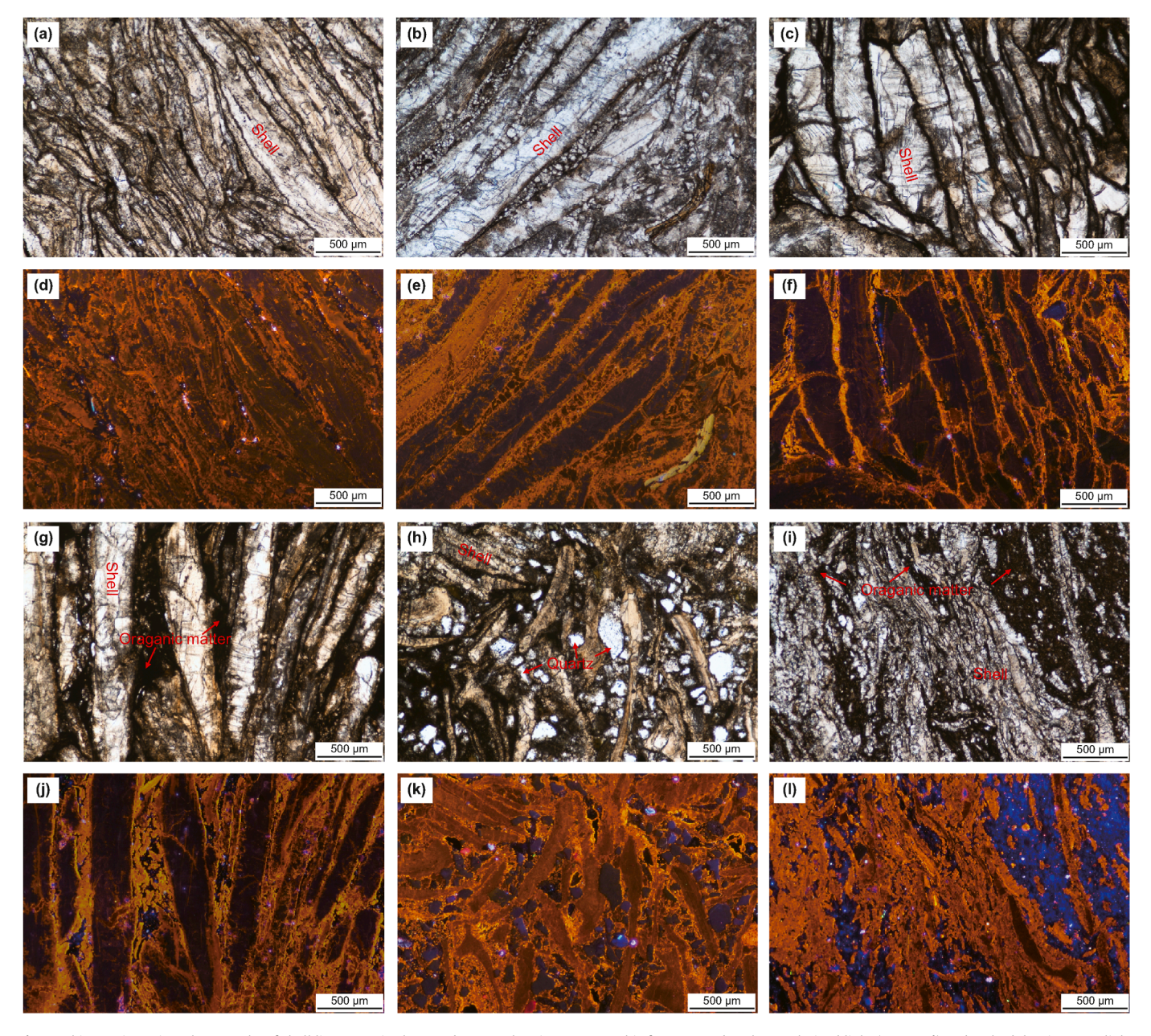


Fig. 2. Thin-section microphotographs of shell limestone in the Yuanba area, showing petrographic features under plane polarized light $(\mathbf{a}-\mathbf{c},\mathbf{g}-\mathbf{i})$ and cathodoluminescent light $(\mathbf{d}-\mathbf{f},\mathbf{j}-\mathbf{l})$. (\mathbf{a},\mathbf{d}) Sample YY2-15, 3879.7 m. (\mathbf{b},\mathbf{e}) Sample YY2-17, 3886.2 m. (\mathbf{c},\mathbf{f}) Sample YY2-22, 3901.9 m. (\mathbf{g},\mathbf{j}) Sample YY2-24, 3909.4 m. (\mathbf{h},\mathbf{k}) Sample YY2-25, 3914.8 m. (\mathbf{i},\mathbf{l}) Sample YB273-7, 4080.4 m. Well preserved shells show dull luminescence $(\mathbf{a}-\mathbf{c},\mathbf{g})$, while partially preserved shells also show dull luminescence (\mathbf{h},\mathbf{i}) . The dark organic matter between shells show light yellow and blue luminescence.

Cretaceous have made it impossible to identify un-eroded strata for correlation in order to restore the surface erosion thickness. Finally, the $R_{\rm o}$ vs. depth method requires systematic $R_{\rm o}$ data at different depth to establish a trend line (Dow, 1977). Vitrinite is rarely found in the Upper Jurassic to Cretaceous red shales because they were deposited under fluvial environments in the Sichuan Basin (Zhai, 1989). Consequently, the $R_{\rm o}$ vs. depth method is also unsuitable to restore the surface erosion thickness in the Sichuan Basin. However, the maximum burial temperature of the J_1z^4 shale can be estimated using the Easy% $R_{\rm o}$ model (Sweeney and Burnham, 1990) and the Δ_{47} solid-state reordering model applied to the J_1z^4 shell limestone. By combining these data with the paleo-temperature gradient established by previous studies, the maximum burial depth of the J_1z^4 shale can be determined.

The surface erosion thickness can then be calculated as the difference between the maximum burial depth and present-day burial depth.

The maximum burial depth can be constrained through combined analysis of maturation of organic matter and solid-state reordering in carbonate minerals. The maturation of a certain source rock or organic matter in the subsurface can be constrained using the classical Easy R_0 model (Sweeney and Burnham, 1990). Organic matter maturation is primarily related to the burial time and thermal history. For a given source rock with measured R_0 value, the general thermal history can be constrained using the Easy R_0 model. The R_0 values of the R_0 value, in the Yuanba area, range from 1.28 to 1.47% (average of 1.36%, Fig. 4), and the corresponding maximum burial temperatures constrained by the Easy R_0 model

Table 1The XRD and cathodoluminescence (CL) of the Jurassic shell limestone samples in the Yuanba area.

Well	Sample ID	Depth, m	Strata	XRD				Sample description	CL of shell
				Calcite	Quartz	Hematite	Clay		
YY2	YY2-15	3879.7	J_1z^4	82.7	12.6	1	2.0	SWP	NCL
YY2	YY2-17	3886.2	J_1z^4	93.6	3.0	3.5	1	SWP	NCL
YY2	YY2-18	3889.4	J_1z^4	97.6	2.4	1	1	SWP	NCL
YY2	YY2-21	3898.0	J_1z^4	93.4	6.6	I	,	SWP	NCL
YY2	YY2-22	3901.9	J_1z^4	83.4	6.4	6.4	3.8	SWP	NCL
YY2	YY2-24	3909.4	J_1z^4	85.1	9.1	3.0	2.8	SWP	NCL
YY2	YY2-25	3914.8	J_1z^4	91.9	7.0	1	1	SPP	WCL
YB273	YB273-1	4072.0	J_1z^4	83.7	10.2	1	4.8	SPP	NCL
YB273	YB273-7	4080.4	J_1z^4	72.4	23.7	1	3.9	SPP	WCL

Note: XRD = X-ray diffraction, SWP = shells' shape well preserved, SPP = shells' shape partially preserved, CL = cathodoluminescence, NCL = non-cathodoluminescence, WCL = weak cathodoluminescence.

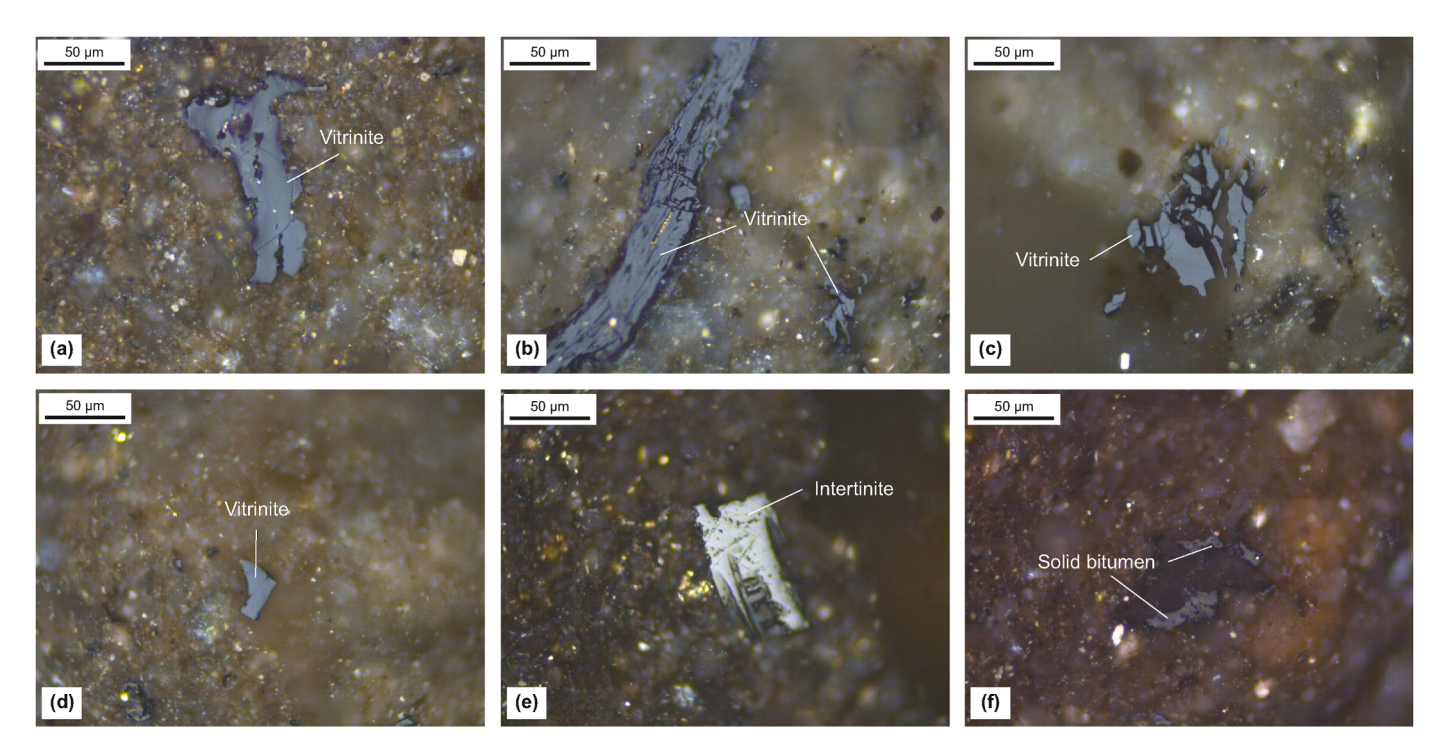


Fig. 3. Microphotographs of main organic constituents in shale samples from the Jurassic Da'anzhai Member in the Yuanba area. (a) Well YY2, 3881.39 m, grey vitrinite. (b) Well YY2, 3882.21 m, grey vitrinite. (c) Well YY2, 3903.71 m, grey vitrinite. (d) Well YY2, 3912.77 m, grey vitrinite. (e) Well YY2, 3885.13 m, light grey intertinite. (f) Well YY2, 3890.95 m, light grey amorphous solid bitumen developed between inorganic minerals.

Table 2 The vitrinite reflectance (R_0) of the Jurassic shale samples from the Yuanba area in the Sichuan Basin.

Sample No.	Area	Well	Depth	Strata	R ₀ , %	Measuring points	±1SD
1	Yuanba	YY2	3881.45	J_1z^4	1.31	22	0.03
2	Yuanba	YY2	3882.63	J_1z^4	1.37	20	0.10
3	Yuanba	YY2	3883.00	J_1z^4	1.33	20	0.09
4	Yuanba	YY2	3883.10	J_1z^4	1.40	22	0.05
5	Yuanba	YY2	3890.95	J_1z^4	1.38	20	0.14
6	Yuanba	YY2	3896.24	J_1z^4	1.31	20	0.02
7	Yuanba	YY2	3899.52	J_1z^4	1.40	23	0.05
8	Yuanba	YY2	3899.64	J_1z^4	1.28	30	0.11
9	Yuanba	YY2	3907.10	J_1z^4	1.34	20	0.03
10	Yuanba	YY2	3907.82	J_1z^4	1.41	23	0.07
11	Yuanba	YY2	3908.70	J_1z^4	1.31	38	0.09
12	Yuanba	YY2	3909.60	J_1z^4	1.41	18	0.08
13	Yuanba	YY2	3910.85	J_1z^4	1.34	20	0.09
14	Yuanba	YY2	3911.60	J_1z^4	1.41	20	0.03
15	Yuanba	YY2	3916.85	J_1z^4	1.30	25	0.03
16	Yuanba	YY2	3917.26	J_1z^4	1.38	35	0.15
17	Yuanba	YY2	3921.74	J_1z^4	1.47	26	0.08

Note: $J_1z^4=$ Jurassic Da'anzhai Member, SD= standard deviation.

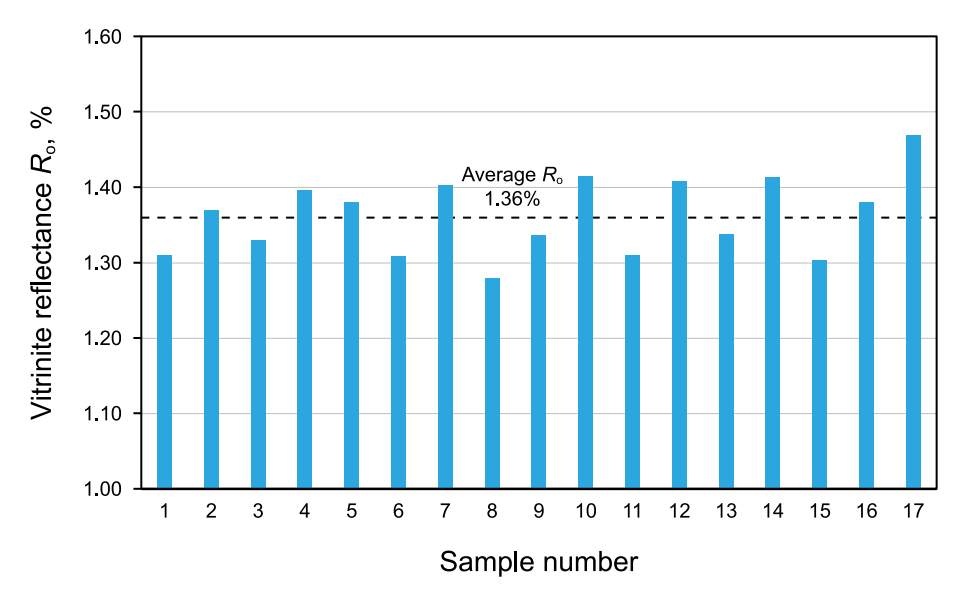


Fig. 4. Vitrinite reflectance (R_0) of shale samples from the well YY2 located in the Jurassic Da'anzhai Member of the Yuanba area.

Table 3 The δ^{18} O, corrected Δ_{47} (CDES90), and $T_{\Delta 47}$ (°C) of the Jurassic shell limestone samples in the Yuanba area, and the reconstructed δ^{18} O of Early Jurassic lake water.

Sample ID	Depth, m	Strata	n	δ ¹³ C (‰, VPDB)	δ ¹⁸ O (‰, VPDB)	Δ47 (CDES90, ‰)	T _{Δ47} , °C (Dennis et al., 2011)	δ ¹⁸ O _{water} (‰, SMOW)
YY2-15	3879.7	J_1z^4	3	3.510 ± 0.006	-14.611 ± 0.010	0.452 ± 0.006	68.5 ± 1.9	-12.19 ± 0.38
YY2-17	3886.2	J_1z^4	3	3.720 ± 0.003	-10.908 ± 0.011	0.464 ± 0.005	65.0 ± 1.4	-9.10 ± 0.29
YY2-18	3889.4	J_1z^4	3	3.460 ± 0.008	-14.481 ± 0.009	0.454 ± 0.004	67.8 ± 1.3	-12.20 ± 0.26
YY2-21	3898.0	J_1z^4	3	4.001 ± 0.003	-13.567 ± 0.012	0.448 ± 0.005	69.7 ± 1.4	-10.88 ± 0.28
YY2-22	3901.9	J_1z^4	3	4.379 ± 0.002	-10.231 ± 0.006	0.466 ± 0.003	64.4 ± 0.8	-8.52 ± 0.17
YY2-24	3909.4	J_1z^4	3	4.159 ± 0.009	-11.008 ± 0.007	0.452 ± 0.005	68.5 ± 1.7	-8.48 ± 0.34
YY2-25	3914.8	J_1z^4	3	3.720 ± 0.002	-14.254 ± 0.009	0.463 ± 0.006	65.0 ± 1.7	-12.55 ± 0.35
YB273-1	4072.0	J_1z^4	3	3.163 ± 0.001	-14.820 ± 0.009	0.450 ± 0.005	69.3 ± 1.7	-12.25 ± 0.34
YB273-7	4080.4	J_1z^4	3	3.327 ± 0.008	-13.757 ± 0.008	0.457 ± 0.003	67.0 ± 0.9	-11.62 ± 0.18

range from 163.5 to 173.5 °C (average of 167.3 °C, Fig. 6). The Δ_{47} solid-state reordering process is influenced by both the time and burial temperature history (Passey and Henkes, 2012; Henkes et al., 2014; Stolper and Eiler, 2015). According to the reported solid-state reordering model, calcite experienced solid-state reordering when the late burial temperature exceeds approximately 100 °C. As a result, the $T_{\Delta 47}$ value deviates from the original formation temperature, and approaches the surrounding temperature when the burial temperature reaches approximatively 200 °C (Henkes et al., 2014; Stolper and Eiler, 2015). For a given calcite sample with a known measured Δ_{47} value and general burial history, the maximum burial temperature can be also constrained using the solid-state reordering model. The $T_{\Delta 47}$ of the J_1z^4 shell limestone is 67.2 \pm 1.4 °C, which is significantly higher than the expected formation temperature of shell limestone and published Early to Middle Jurassic temperature estimates (25–35°C, Suan et al., 2010; Rosales et al., 2004). The formation temperature of biological shells (e.g., bivalve, brachiopod, foraminifera, etc.) is generally in equilibrium with the temperature of their surrounding environment (Came et al., 2014; Wang et al., 2016b; Dong et al., 2021), such as lake or sea water temperature where these organisms lived. However, the clumped isotope of some carbonate materials (e.g., cavefilled carbonates, skeletal calcites, and microbially-involved carbonates) do not always reach equilibrium ($T_{\Delta 47}$ is different from $T_{\Delta 48}$), meaning that the $T_{\Delta 47}$ may not represent environmental

temperature (Bajnai et al., 2020). This clumped isotope disequilibrium is mainly related to CO_2 hydration, hydroxylation, and CO_2 degassing (Guo, 2020). Because no published studies have reported this problem in brachiopods and bivalves, we assume in this study that the J_1z^4 shell temperatures are considered representative of the environmental temperatures. In the Sichuan Basin, for the shell limestone which has reached clumped isotope equilibrium, the relatively high $T_{\Delta 47}$ of the J_1z^4 shell limestones suggests that they most probably underwent solid-state reordering or recrystallization during late burial.

Although a few shells show local cleavage cracks (Fig. 2(a)) suggesting limited recrystallization, most shells or shells' fragments show no or limited cathodoluminescence (Fig. 2). Additionally, the $T_{\Delta47}$ values across all samples show no significant differences (Fig. 5). Furthermore, no linear relationship between the $T_{\Delta47}$ and δ^{18} O can be observed in shell limestones (Fig. 7), suggesting limited diagenetic alteration. Therefore, both petrographic observations, $T_{\Delta47}$ and δ^{18} O values of shell limestones suggest that no significant recrystallization or late diagenetic alteration occurred in the J_1z^4 shell limestone in the Yuanba area. Consequently, the relatively high $T_{\Delta47}$ of the J_1z^4 shell limestone was mainly caused by the solid-state reordering. In addition, the maximum burial temperature determined by the Easy% R_0 model (167.3 °C) exceeds the threshold temperature (100 °C) for solid-state reordering. Therefore, a solid-state reordering model can be

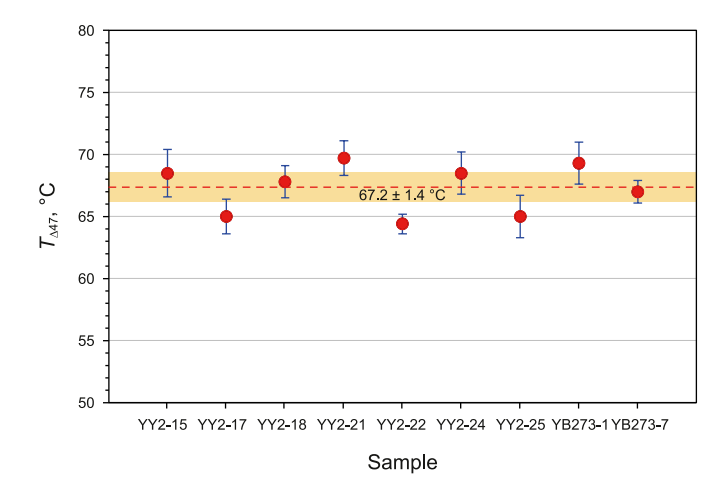


Fig. 5. Temperature estimations using clumped isotope ($T_{\Delta 47}$) of shell limestone samples from the Jurassic Da'anzhai Member in the Yuanba area. The red dashed line represents the average $T_{\Delta 47}$ (67.2 °C), and the yellow shadow shows average error of all samples (± 1.4 °C).

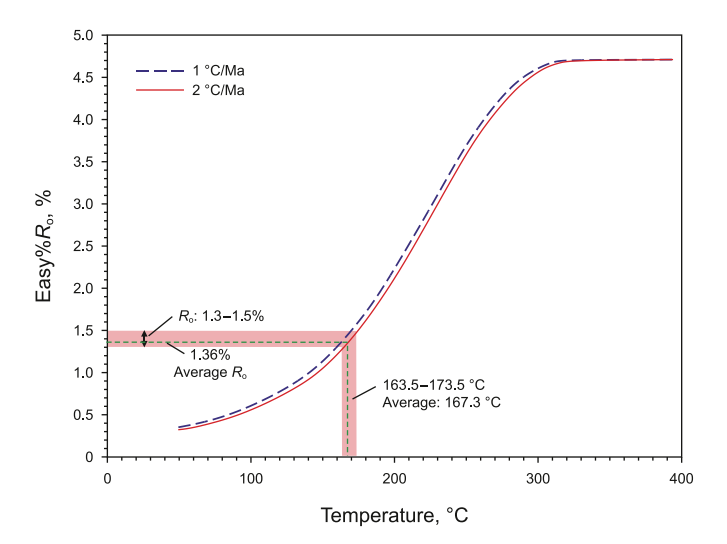


Fig. 6. Vitrinite reflectance (R_0) vs. temperature based on the Easy $\%R_0$ model (Sweeney and Burnham, 1990). The green dashed line shows the average R_0 (1.36%) and its corresponding average maximum burial temperature (167.3 °C).

used to constrain the maximum burial temperature of the J_1z^4 shell limestone in the Yuanba area.

Several studies have investigated solid-state reordering in carbonate clumped isotopes (Passey and Henkes, 2012; Henkes et al., 2014; Stolper and Eiler, 2015; Lloyd et al., 2018). Solidstate reordering refers to the diffusion of C-O bond through solid mineral lattice (Passey and Henkes, 2012). Passey and Henkes (2012) were the first to study Δ_{47} solid-state reordering and determined the Arrhenius parameters for solid-state reordering, assuming that the reaction follows a first-order rate law. However, subsequent research found that the initial reordering does not follow a first-order reaction. To address this issue, Henkes et al. (2014) proposed the transient defect/equilibrium defect model, which accounts for both initial non-first-order reaction and late first-order reaction. By extrapolating kinetics measured at elevated temperatures to those at lower temperatures, they obtained nearly identical kinetics for calcite, brachiopod and optical calcites. Stolper and Eiler (2015) proposed the exchange-diffusion model, which incorporates both diffusion of isotopes and isotope-

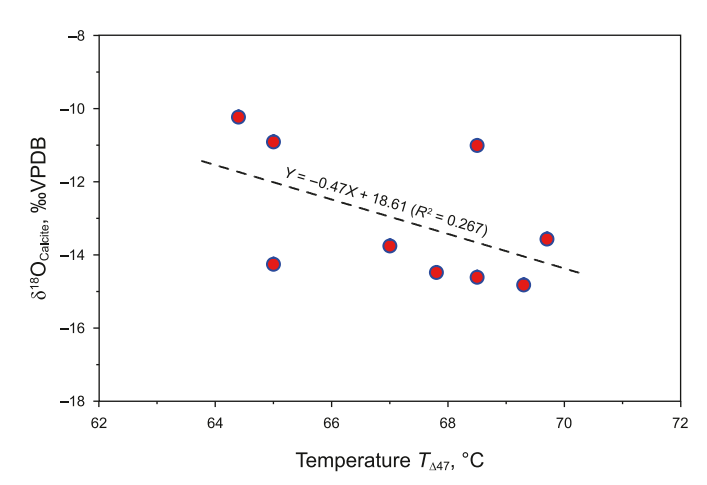


Fig. 7. Clumped isotopes temperature $(T_{\Delta 47})$ vs. δ^{18} O of shell limestones from the Jurassic Da'anzhai Member in the Yuanba area.

exchange reaction. This model allows a better fit of the reaction kinetics capturing both the initial and later stage of reordering. As a result, the exchange-diffusion model is now widely accepted and used by the scientific community (Stolper and Eiler, 2015; Lloyd et al., 2018; Li et al., 2020; Ryb et al., 2021) and is used in this study.

The initial formation temperature and geological age of carbonate samples are essential input parameters for running the solid-state reordering models (Stolper and Eiler, 2015). The geological age of the J_1z^4 sample in the Sichuan Basin is 180.3 ± 3.2 Ma determined by the Re-Os isochron of the I_1z^4 shale (Xu et al., 2017b). If the initial formation temperatures of the I_1z^4 shell limestone were assumed to be 20, 25, 28, 30, and 35 °C, the corresponding maximum burial temperature determined by the solid-state reordering model are 120, 140, 168, 188, and 196 °C, respectively (Fig. 8). Compared with the maximum burial temperature determined by the Easy%R₀ model (about 167.3 °C, Fig. 6), the initial formation temperature of the shell limestone is around 28 °C. The I_1z^4 shell limestone was formed by the accumulation of biological shells and fragments, which were deposited in an inshore shallow lake water in the Sichuan Basin (Wang et al., 2020). Therefore, the temperatures of these shells are similar to the average temperature of the J_1z^4 lake water.

The paleolatitude and paleolongitude of the Jurassic lake in the Sichuan Basin at 179 Ma were approximatively 40° N and 130–140° E, respectively (Xu et al., 2017b). Jin et al. (2024) reconstructed the terrestrial temperatures during the Middle Jurassic in the Sichuan Basin (30–35° N) using clumped isotope of carbonate nodules in paleo soils, and reporting annual temperatures ranging from 30 \pm 4 to 34 \pm 4 °C, which are slightly higher than the Early Jurassic temperature determined in our study. This is consistent with the expected trend of increase temperature from Early Jurassic to Early Cretaceous (Suan et al., 2010). In addition, the Early Jurassic seawater temperature could reach up 25 °C in the Basque-Cantabrian Basin (25° N) (Rosales et al., 2004). The relatively high temperature in Early Jurassic was related to the T-OAE, during which the atmospheric CO2 concentrations was high and corresponding to a typical greenhouse climate. Thus, the initial formation temperature of the shell limestone or lake water temperature determined in this study (i.e., ~28 °C) is consistent with geological and climatic reconstructions.

Using the reported age, the determined initial formation temperature and maximum burial temperature of the J_1z^4 shell limestone, the solid-state reordering model can be run again to obtain the final predicted equilibrium $T_{\Delta 47}$. As shown in Fig. 8, the

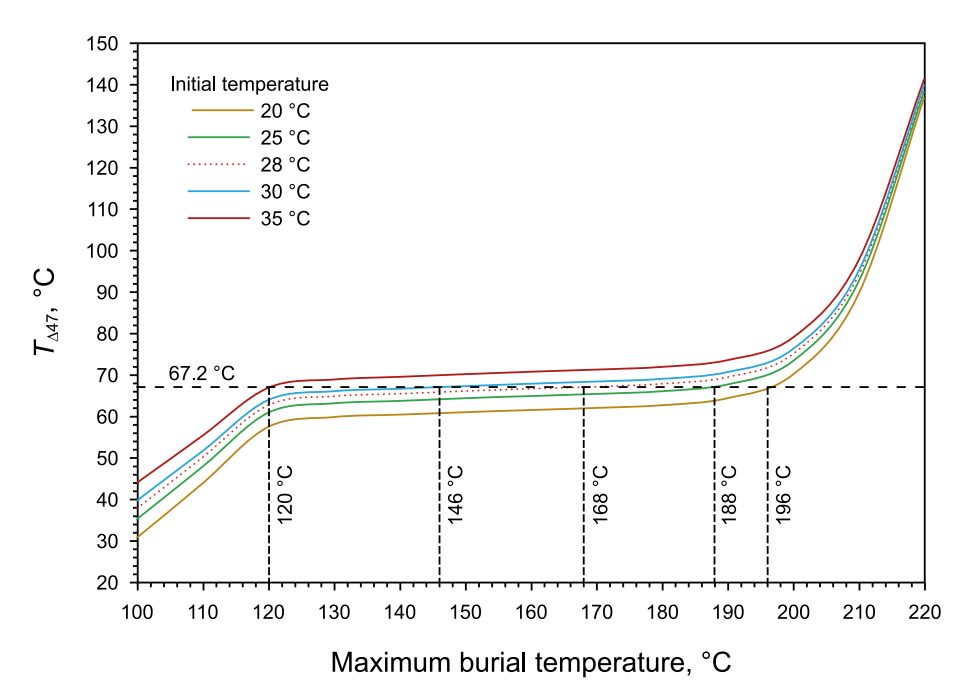


Fig. 8. Final clumped isotopes temperature ($T_{\Delta 47}$) vs. the maximum burial temperature of the J_1z^4 shell limestone in the Yuanba area, assuming that shells crystalized at 20, 25, 28, 30, and 35 °C at 180 Ma using Stolper and Eiler's (2015) solid-state reordering model.

final predicted $T_{\Delta47}$ shows slight variations depending on the late-stage cooling in the thermal history, even when the maximum burial temperature remains the same. The final $T_{\Delta47}$ is 67.3 °C for a three-stages temperature decrease (Fig. 9(a)) and 66.8 °C for a single temperature decrease since 100 Ma (Fig. 9(b)). The late uplift and denudation can be divided into three stages since the Late Cretaceous (Deng et al., 2013), leading to a more reasonable three-stages temperature decrease for the solid-state reordering model. When the maximum burial temperature was assumed to be 170 °C, the final predicted $T_{\Delta47}$ (67.3 °C, Fig. 9(a)) is in good agreement with the $T_{\Delta47}$ of the J₁z⁴ shell limestone (67.2 ± 1.4 °C,

Fig. 5). As a result, the most probable maximum burial temperature of the I_1z^4 shell limestone in the Yuanba area is ~170 °C.

Taken together, based on the organic matter maturity model (Easy% R_{o}) and solid-state reordering model, the maximum burial temperature of the $J_{1}z^{4}$ in the Yuanba area is estimated at ~170 °C (Figs. 6 and 9(a)). The paleo-temperature gradient of the Early Jurassic in the northern Sichuan Basin is about 2.63 °C/100 m (Zhu et al., 2016). Based on this gradient and estimated maximum burial temperature, the maximum burial depth of the $J_{1}z^{4}$ in the Yuanba area can be calculated to be about 5400 m. The difference between the maximum burial depth and present-day burial depth (about

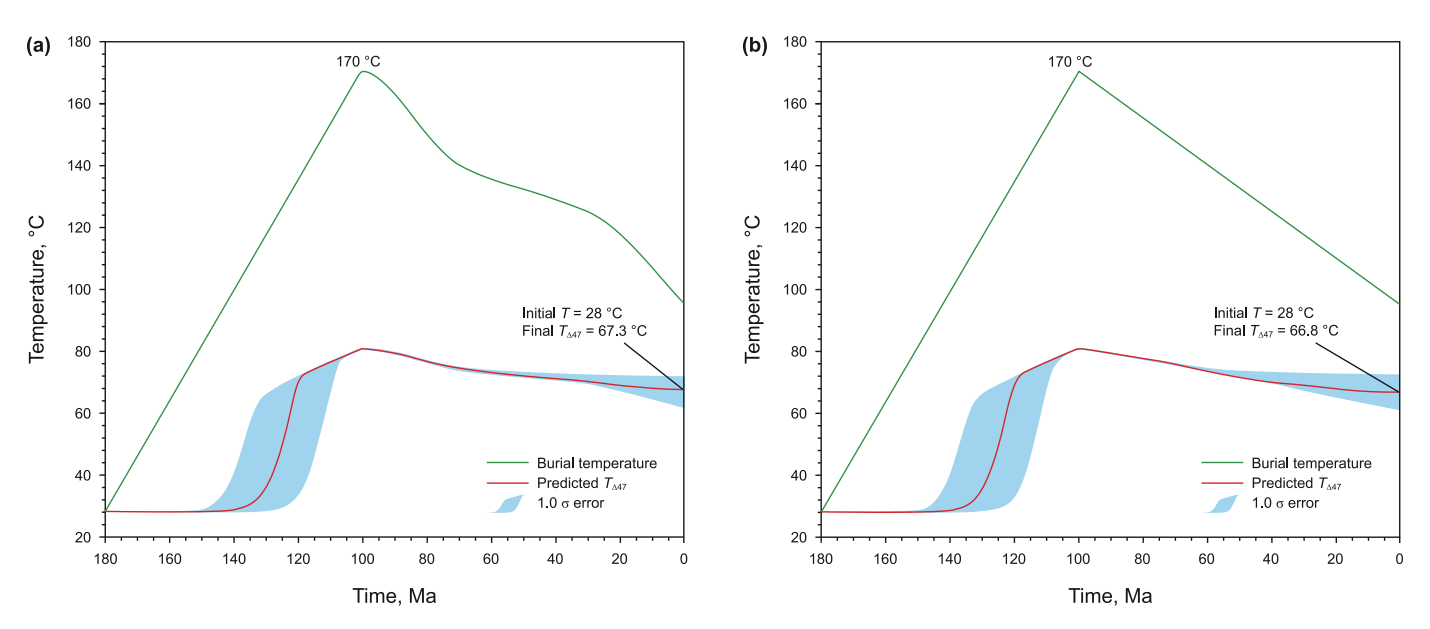


Fig. 9. Clumped isotope temperature ($T_{\Delta 47}$) evolution of the J_1z^4 shell limestone from the Yuanba area, assuming that the shell crystalized at 28 °C at 180 Ma and that the maximum burial temperature reached 170 °C at 100 Ma and then decreased to 95 °C during late uplift. (**a**) A three-stages' temperature decreasing with a final predicted $T_{\Delta 47}$ of 67.3 °C; (**b**) A single temperature decreasing with a final predicted $T_{\Delta 47}$ of 66.8 °C. Note that $T_{\Delta 47}$ of shell limestone increased about 39.3 °C due to the solid-state reordering.

3900, Table 2) is about 1500 m, which represents the most probable surface erosion thickness for the Yuanba area. The burial history and thermal evolution were built using the software PetroMod 11 (Fig. 10(a)) based on the determined maximum burial temperature and surface erosion thickness. The predicted $R_{\rm o}$ value of the $J_{\rm 1}z^{\rm 4}$ shale fit the measured $R_{\rm o}$ (Fig. 10(b)), suggesting the reconstructed surface erosion thickness was reasonable in this study. This study provides a potential new approach for reconstructing the surface erosion thickness by integrating an organic matter maturity model with a solid-state reordering model. However, converting the maximum burial temperature to the maximum burial depth relies on the study of paleo-temperature gradients.

5.2. Solid-state reordering of shell limestone and $\delta^{18}{\rm O}$ of the early Jurassic lake water

A large number of studies have been conducted on δ^{18} O of global seawater leading to the establishment of a relatively complete δ^{18} O evolution curve since the Phanerozoic (Veizer et al., 1997, 1999; Veizer and Prokoph, 2015). In contrast, δ^{18} O of lake water is more variable, making it more difficult to establish a uniform evolution curve (Hladyniuk and Longstaffe, 2016; Haig et al., 2021). To constrain δ^{18} O of lake water using conventional oxygen isotope thermometer, both the δ^{18} O values and initial formation temperatures of unaltered lacustrine fossils have to be determined. The δ^{18} O values of lacustrine fossils can be easily measured and the initial formation temperature can be constrained combined using the Easy% R_0 and the solid-state reordering model. The average initial formation temperatures of the J_1z^4 shell limestone, determined using solid-state reordering, is about 28 °C (Fig. 8). Due to solid-state reordering, the $T_{\Delta 47}$ of the shell

limestone has increased of about 39.2 °C (67.2 °C minus 28 °C). As a result, the initial equilibrium temperature of each shell limestone samples can be calculated by subtracting 39.2 °C from its present-day $T_{\Delta47}$ value.

Based on the reconstructed initial equilibrium temperature and oxygen isotopes of shell limestone samples, the δ^{18} O of the Early Jurassic lake water in the Yuanba area can be determined using the conventional oxygen isotope thermometer (Kim and O'Neil, 1997). As shown in Fig. 11, the δ^{18} O values of the Early Jurassic lake water in the Yuanba area range from -12.55% to -8.48% (average of -10.8%), which are significantly lower than those of co-eval seawater (about -3.0%, Veizer and Prokoph, 2015). The $\delta^{18}O$ value of formation water in reddish paleo-soils can be as low as -6.3% during the Middle Jurassic in the Sichuan Basin (Jin et al., 2024). The δ^{18} O value of the Early Jurassic lake water in the Sichuan Basin should be much lower than -6.3% due to deeper water with more meteoric water input. Additionally, the $\delta^{18}O$ values of natural lake water in western United States and Lake Onega Basin can range from -20.0% to -10.0% (Henderson and Shuman, 2009) and -11.5% to -9.3% (Borodulina et al., 2023), respectively. Therefore, the δ^{18} O value of the Early Jurassic lake water (average of -10.8%) determined in this study is consistent with global lacustrine isotope variations.

The δ^{18} O value of lake water is mainly controlled by the balance between freshwater input and evaporation (Gibson et al., 2016). The oxygen isotope composition of the Early Jurassic lake water in the Sichuan Basin (-12.55% to -8.48%, SMOW) indicate that freshwater input during this period was significantly higher than the evaporation, resulting in oxygen isotope value significantly lower than those of the co-eval seawater (about -3.0%, Veizer and Prokoph, 2015). Combined with the initial formation temperatures of the J₁z⁴ shell limestone (about 28 °C) discussed above, these

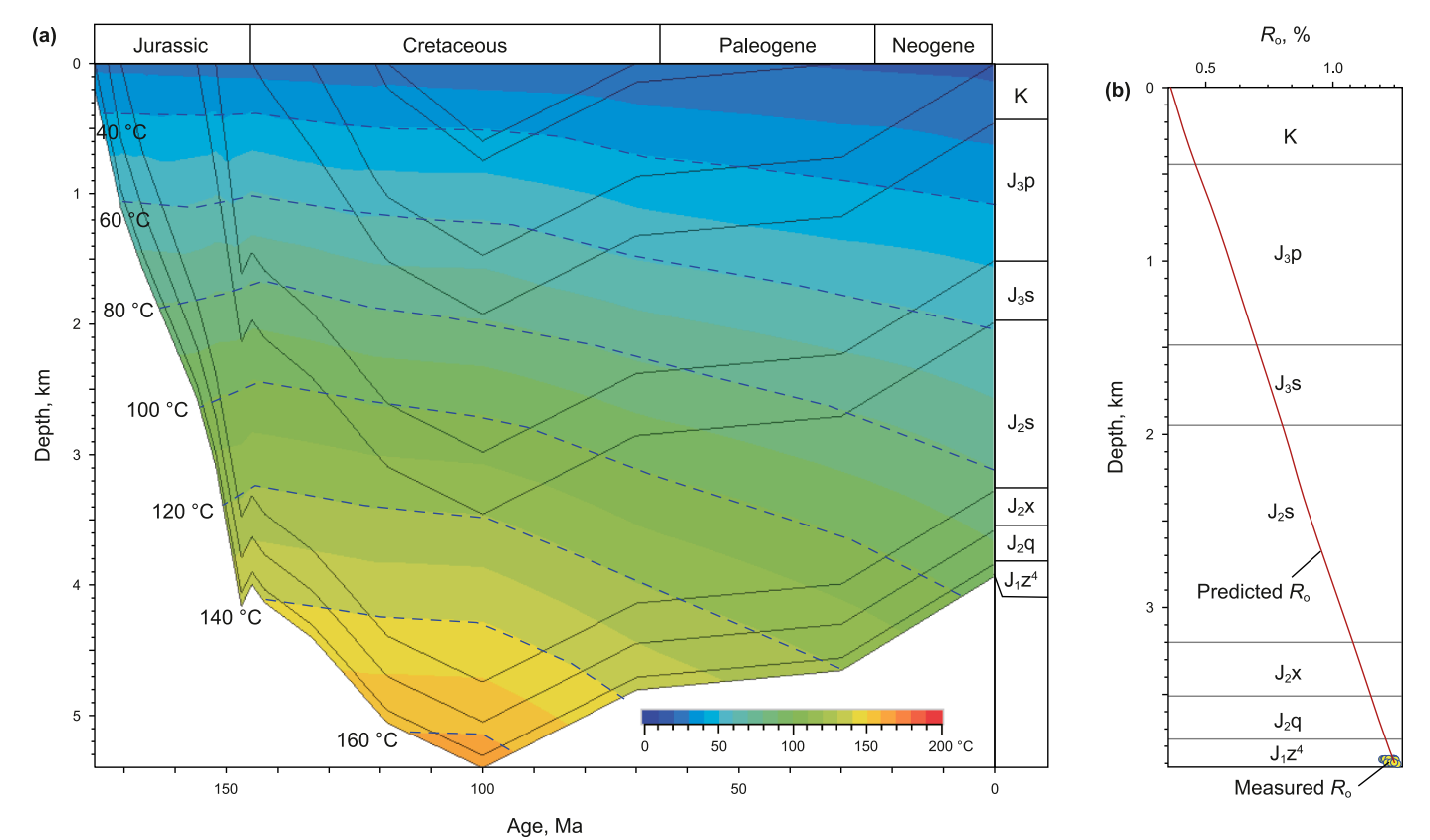


Fig. 10. (a) Burial and exhumation temperature history of the well YY2 using the software of PetroMod 11, based on the maximum burial temperature determined by clumped isotopes of shell limestone. (b) Predicted R_0 and measured R_0 of the J_1z^4 shale of the well YY2.

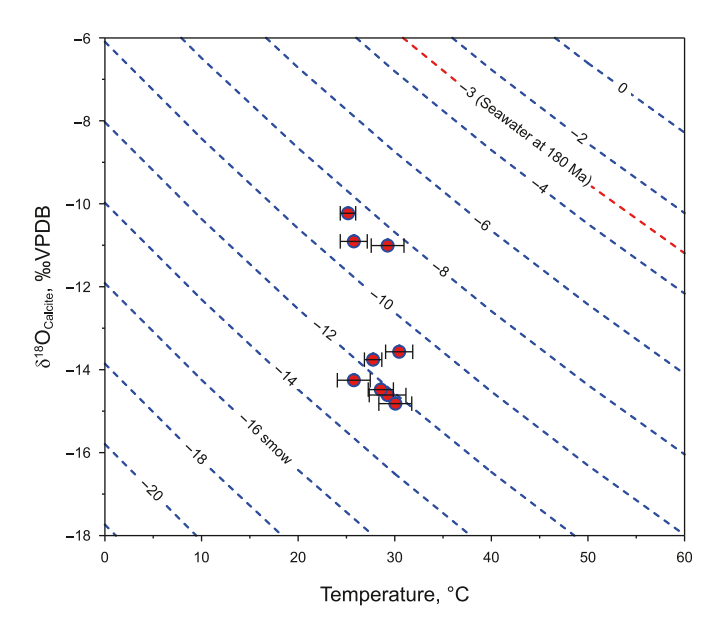


Fig. 11. Oxygen isotopes (δ^{18} O, SMOW) of the Early Jurassic lake water based on the restored clumped isotope ($T_{\Delta47}$) and δ^{18} O (VPBD) of the J₁z⁴ shell limestone samples in the Yuanba area based on Kim and O'Neil's (1997) equation: 10^3 Inα_{calcite-water} = 18.03×10^3 / T-32.42. The restored $T_{\Delta47}$ was calculated by present $T_{\Delta47}$ minus 39.3 °C determined by the solid-state reordering model in Fig. 9. The red dashed line represents δ^{18} O of the lurassic seawater (about -3.0%, SMOW) at 180 Ma in the South China Block.

findings suggest that the climate during the Early Jurassic in the Sichuan Basin was warm and humid conditions that were favorable for the production of organic matter and the formation of organic-rich shales. This is consistent with the discovery of several sets of shales in the Lower Jurassic of the Sichuan Basin (Xu et al., 2017a). Trace elements analyses of the lacustrine J_1z^4 shales also suggested that the J_1z^4 shales were mainly developed in a warm and fresh water environment (Xu et al., 2017a). Furthermore, the $\delta^{18}\text{O}$ values of Early Jurassic lake water, as determined in this study, appear to cluster around two distinct end-member compositions (Fig. 11): -8.7% and -12.0% (SMOW). This variation in oxygen isotope likely reflects paleoclimate fluctuation during the Early Jurassic (Xu et al., 2017a, 2017b). The oxygen isotope of the Jurassic lake water, reconstructed from the Δ_{47} of shell limestone, is consistent with the paleoenvironmental condition in which the co-existing lacustrine shales were developed. This finding further validates the reliability of lake water δ^{18} O values reconstructed from Δ_{47} measurements in shell limestones, while establishing a robust framework for determining paleo-lacustrine oxygen isotope compositions.

Lacustrine shales are widely developed in the l_1z^2 , l_1z^3 and l_1z^4 formations, with many layers of shell limestone developed in these co-existing shales in the Sichuan Basin (Liu et al., 2020). Systematic studies on the Δ_{47} of these shell limestones are expected to reveal variations in the oxygen isotope of the Early Jurassic lake water and possible climatic changes in the Sichuan Basin. This research provides fundamental constraints on the development mechanisms and distribution predictions of the Lower Jurassic shales. In particular, the reconstructed oxygen isotopes of the Early Jurassic lake water can provide fluid information for calcite veins development in the Lower Jurassic shales. Consequently, the formation temperature and diagenetic stages of these calcite veins can be determined using the conventional oxygen isotope thermometer. This approach is expected to be valuable for shale gas exploration and development in the Lower Jurassic of the Sichuan Basin.

6. Conclusions

This study provides a geologic case study for using Δ_{47} analysis of well-preserved shell limestones to reconstruct erosion thickness and the δ^{18} O of Early Jurassic lake water in the Sichuan Basin. The main findings are summarized as follows.

- (1) The J₁z⁴ shell limestones in the Yuanba area can be classified into two types based on shells' shape: well-preserved and partially preserved shell limestones. Both types show no significant recrystallization and lack cathodoluminescence, suggesting that the shell limestones did not experience significant late diagenetic alteration.
- (2) The $T_{\Delta47}$ values of the J_1z^4 shell limestones range from 64.4 \pm 0.8 to 69.7 \pm 1.4 °C (average 67.2 \pm 1.4 °C), significantly higher than the estimated paleotemperature of the Early Jurassic. This discrepancy indicates that the shell limestones experienced solid-state reordering during burial. Therefore, the $T_{\Delta47}$ value does not reflect the initial formation temperature of the shell limestone.
- (3) The maximum burial temperature of the J_1z^4 in the Yuanba area was about 170 °C, integrating the organic matter's mature model (Easy% R_0) and the calcite's solid-state reordering model. Based on the paleotemperature gradient, the surface erosion thickness during late uplift is about 1500 m in the Yuanba area.
- (4) The initial formation temperature of the J_1z^4 shell limestone is determined to be 28 °C using Δ_{47} solid-state reordering model. The calculated δ^{18} O of the Early Jurassic lake water range from -10.8% to -8.0% (SMOW), suggesting a dominance of fresh meteoric water input over evaporation. These results collectively indicate a warm and humid Early Jurassic climate in the Sichuan Basin, which was favorable for the formation of organic-rich lacustrine shales.

CRediT authorship contribution statement

Ping-Ping Li: Writing – original draft, Methodology, Investigation, Conceptualization. **Shi-Jie He:** Resources, Methodology. **Zhan-Jie Xu:** Resources, Methodology. **Dai-Qin Jiang:** Resources. **Hua-Yao Zou:** Supervision. **Fang Hao:** Project administration.

Declaration of competing interest

The authors declare that they have no known competing financial interests or personal relationships that could have appeared to influence the work reported in this paper.

Acknowledgments

This study was supported by National Natural Science Foundation of China (42372148). Special thanks are given to the SINOPEC Exploration Company for samples collection, and Linlin Cui at the Institute of Geology and Geophysics (Chinese Academy of Sciences) for clumped isotopes measurement, and Thomas Bernard for linguistic assistance. Sincere thanks are extended to the four anonymous reviewers whose comments significantly improved the quality of the paper.

Appendix A. Supplementary data

Supplementary data to this article can be found online at https://doi.org/10.1016/j.petsci.2025.05.030.

References

- Bajnai, D., Guo, W., Spötl, C., Coplen, T.B., Methner, K., Löffler, N., Krsnik, E., Gischler, E., Hansen, M., Henkel, D., Price, G.D., Raddatz, J., Scholz, D., Fiebig, J., 2020. Dual clumped isotope thermometry resolves kinetic biases in carbonate formation temperatures. Nature Communication 11, 4005. https://doi.org/10.1038/s41467-020-17501-0
- Banerjee, S., Ghosh, P., Banerjee, Y., Riding, R., 2023. Oxygen isotopic composition of Paleoproterozoic seawater revealed by clumped isotope analysis of dolomite, Vempalle Formation, Cuddapah, India. Chem. Geol. 621, 121356. https://doi.org/10.1016/j.chemgeo.2023.121356.
- Bernasconi, S.M., Müller, I.A., Bergmann, K.D., Breitenbach, S.F.M., Fernandez, A., Hodell, D.A., Jaggi, M., Meckler, A.N., Millan, I., Ziegler, M., 2018. Reducing uncertainties in carbonate clumped isotope analysis through consistent carbonate-based standardization. Geochem. Geophys. Geosystems 19, 2895–2914. https://doi.org/10.1029/2017GC007385.
- Borodulina, G., Tokarev, I., Yakovlev, E., 2023. Isotope composition of natural water in Lake Onega Basin. Water 15, 1855. https://doi.org/10.3390/w15101855.
- Came, R.E., Brand, U., Affek, H.P., 2014. Clumped isotope signatures in modern brachiopod carbonate. Chem. Geol. 377, 20–30. https://doi.org/10.1016/j. chemgeo.2014.04.004.
- Cummins, R.C., Finnegan, S., Fike, D.A., Eiler, J.M., Fischer, W.W., 2014. Carbonate clumped isotope constraints on Silurian ocean temperature and seawater s¹⁸0. Geochem. Cosmochim. Acta 140, 241–258. https://doi.org/10.1016/j.gca.2014.05.024.
- Deng, B., Liu, S.G., Li, Z.W., Jansa, L., Liu, S., Wang, G.Z., Sun, W., 2013. Differential exhumation at eastern margin of Tibetan Plateau, from apatite fission-track thermochronology. Tectonophysics 591, 98–115. https://doi.org/10.1016/j.tecto.2012.11.012.
- Dennis, K.J., Affek, H.P., Passey, B.H., Schrag, D.P., Eiler, J.M., 2011. Defining an absolute reference frame for 'clumped' isotope studies of CO₂. Geochem. Cosmochim. Acta 75, 7117–7131. https://doi.org/10.1016/j.gca.2011.09.025.
- Dong, J.B., Eiler, J., An, Z.S., Li, X.Z., Liu, W.G., Hu, J., 2021. Clumped isotopic compositions of cultured and natural land-snail shells and their implications. Palaeogeogr. Palaeoclimatol. Palaeoecol. 577, 110530. https://doi.org/10.1016/j.palaeo.2021.110530.
- Dow, W.G., 1977. Kerogen studies and geological interpretations. J. Geochem. Explor. 7, 79–99.
- Eagle, R.A., Schauble, E.A., Tripati, A.K., Tütkend, T., Hulberte, R.C., Eiler, J.M., 2010. Body temperatures of modern and extinct vertebrates from ¹³C-¹⁸O bond abundances in bioapatite. Proceedings of the National Academy of Sciences of the United States of America 107, 10377–10382. https://doi.org/10.1073/pnas.0911115107
- Eiler, J.M., 2007. "Clumped-isotope" geochemistry: The study of naturally-occurring, multiply-substituted isotopologues. Earth Planet Sci. Lett. 262, 309–327. https://doi.org/10.1016/j.epsl.2007.08.020.
- English, K.L., Redfern, J., Corcoran, D.V., English, J.M., Cherif, R.Y., 2016. Constraining burial history and petroleum charge in exhumed basins: new insights from the Illizi Basin, Algeria. AAPG (Am. Assoc. Pet. Geol.) Bull. 100, 623–655. https://doi. org/10.1306/12171515067.
- Ferry, J.M., Passey, B.H., Vasconcelos, C., Eiler, J.M., 2011. Formation of dolomite at 40-80 °C in the Latemar carbonate buildup, Dolomites, Italy, from clumped isotope thermometry. Geology 39, 571-574. https://doi.org/10.1130/G31845.1.
- Ghosh, P., Adkins, J., Affek, H., Balta, B., Guo, W.F., Schauble, E.A., Schrag, D., Eller, J. M., 2006. ¹³C-¹⁸O bonds in carbonate minerals: A new kind of paleothermometer. Geochem. Cosmochim. Acta 70, 1439–1456. https://doi.org/10.1016/j.gca.2005.11.014.
- Gibson, J.J., Birks, S.J., Yi, Y., 2016. Stable isotope mass balance of lakes: a contemporary perspective. Quat. Sci. Rev. 131, 316–328. https://doi.org/ 10.1016/j.quascirev.2015.04.013.
- Guo, W., 2020. Kinetic clumped isotope fractionation in the DIC-H₂O-CO₂ system: patterns, controls, and implications. Geochem. Cosmochim. Acta 268, 230–257. https://doi.org/10.1016/j.gca.2019.07.055.
- Guo, Y.R., Deng, W.F., Liu, X., Kong, K., Yan, W., Wei, G.J., 2021. Clumped isotope geochemistry of island carbonates in the South China Sea: implications for early diagenesis and dolomitization. Mar. Geol. 437, 106513. https://doi.org/ 10.1016/j.margeo.2021.106513.
- Haig, H.A., Hayes, N.M., Simpson, G.L., Yi, Y., Wissel, B., Hodder, K.R., Leavitt, P.R., 2021. Effects of seasonal and interannual variability in water isotopes (δ²H, δ¹⁸O) on estimates of water balance in a chain of seven prairie lakes. J. Hydrol. X 10, 100069. https://doi.org/10.1016/j.hydroa.2020.100069.
- Heasler, H.P., Kharitonova, N.A., 1996. Analysis of sonic well logs applied to erosion estimates in the Bighorn Basin, Wyoming. AAPG (Am. Assoc. Pet. Geol.) Bull. 80, 630–646. https://doi.org/10.1306/64ED885E-1724-11D7-864500010 2C1865D.
- Hemingway, J.D., Henkes, G.A., 2021. A disordered kinetic model for clumped isotope bond reordering in carbonates. Earth Planet Sci. Lett. 566, 116962. https://doi.org/10.1016/j.epsl.2021.117191.
- Henderson, A.K., Shuman, B.N., 2009. Hydrogen and oxygen isotopic compositions of lake water in the western United States. GSA Bull. 121, 1179–1189.
- Henkes, G.A., Passey, B.H., Grossman, E.L., Shenton, B.J., Pérez-Huerta, A., Yancey, T. E., 2014. Temperature limits for preservation of primary calcite clumped isotope paleotemperatures. Geochem. Cosmochim. Acta 139, 362–382. https://doi.org/10.1016/j.gca.2014.04.040.

Henkes, G.A., Passey, B.H., Grossman, E.L., Shenton, B.J., Yancey, T.E., Pérez-Huerta, A., 2018. Temperature evolution and the oxygen isotope composition of Phanerozoic oceans from carbonate clumped isotope thermometry. Earth Planet Sci. Lett. 490, 40–50. https://doi.org/10.1016/j.epsl.2018.02.001.

- Hladyniuk, R., Longstaffe, F.J., 2016. Oxygen-isotope variations in post-glacial lake ontario. Quat. Sci. Rev. 134, 39–50. https://doi.org/10.1016/j. quascirev.2016.01.002.
- Holmes, J., Burn, M., Cisneros-Dozal, L.M., Jones, M., Metcalfe, S., 2023. An 1800-year oxygen-isotope record of short- and long-term hydroclimate variability in the northern neotropics from a Jamaican marl lake. Quat. Sci. Rev. 301, 107930. https://doi.org/10.1016/j.guascirev.2022.107930.
- Horita, J., 2014. Oxygen and carbon isotope fractionation in the system dolomite-water-CO₂ to elevated temperatures. Geochem. Cosmochim. Acta 129, 111–124. https://doi.org/10.1016/j.gca.2013.12.027.
- Huntington, K.W., Eiler, J.M., Affek, H.P., Guo, W.F., Bonifacie, M., Yeung, L.Y.,
 Thiagarajan, N., Passey, B., Tripati, A., Daeron, M., Came, R., 2009. Methods and limitations of 'clumped' CO₂ isotope (Δ₄₇) analysis by gas-source isotope ratio mass spectrometry. J. Mass Spectrom. 44 (9), 1318–1329. https://doi.org/10.1002/jms.1614.
- Jaffrés, J.B.D., Shields, G.A., Wallmann, K., 2007. The oxygen isotope evolution of seawater: A critical review of a long-standing controversy and an improved geological water cycle model for the past 3.4 billion years. Earth Sci. Rev. 83, 83–122. https://doi.org/10.1016/j.earscirev.2007.04.002.
 Jiang, D., Li, P., Zheng, M., Chen, Q., Xiong, W., Zou, H., 2023. Impacts of different
- Jiang, D., Li, P., Zheng, M., Chen, Q., Xiong, W., Zou, H., 2023. Impacts of different matrix components on multi-scale pore structure and reservoir capacity: insights from the Jurassic Da'anzhai member in the Yuanba area, Sichuan Basin. Energy Rep. 9, 1251–1264. https://doi.org/10.1016/j.egyr.2022.12.020.
- Jin, T., Huntington, K.W., Wen, Y., Gu, X., Schauer, A.J., Zhang, L., 2024. Clumped isotope records of terrestrial temperatures during the Middle Jurassic (180–150 Ma) in East China. Palaeogeogr. Palaeoclimatol. Palaeoecol. 637, 112014. https://doi.org/10.1016/j.palaeo.2024.112014.
- Kim, S.T., O'Neil, J.R., 1997. Equilibrium and nonequilibrium oxygen isotope effects in synthetic carbonates. Geochem. Cosmochim. Acta 61, 3461–3475. https:// doi.org/10.1016/S0016-7037(97)00169-5.
- Li, P., Hao, F., Guo, X., Zou, H., Yu, X., Wang, G., 2015. Processes involved in the origin and accumulation of hydrocarbon gases in the Yuanba gas field, Sichuan Basin, Southwest China. Mar. Petrol. Geol. 59, 150–165. https://doi.org/10.1016/j.marpetgeo.2014.08.003.
- Li, Y., He, D., Chen, L., Mei, Q., Li, C., Zhang, L., 2016. Cretaceous sedimentary basins in Sichuan, SW China: Restoration of tectonic and depositional environments. Cretac. Res. 57, 50–65. https://doi.org/10.1016/j.cretres.2015.07.013.
- Li, P., Zou, H., Hao, F., Yu, X., Wang, G., Eiler, J.M., 2020. Using clumped isotopes to determine the origin of the Middle Permian Qixia Formation dolostone, NW Sichuan Basin, China. Mar. Petrol. Geol. 122, 104660. https://doi.org/10.1016/j. marpetgeo.2020.104660.
- Li, P., Duan, J., Cheng, Z., Zou, H., 2021. Using clumped isotopes to reconstruct the maximum burial temperature: A case study in the Sichuan Basin. Front. Earth Sci. 9, 759372. https://doi.org/10.3389/feart.2021.759372.
- Liu, Z., Liu, G., Hu, Z., Feng, D., Zhu, T., Bian, R., Jiang, T., Jin, Z., 2020. Lithofacies types and assemblage features of continental shale strata and their implications for shale gas exploration: A case study of the Middle and Lower Jurassic strata in the Sichuan Basin. Nat. Gas. Ind. B 7, 358–369. https://doi.org/10.1016/ i.ngib.2019.12.004.
- Liu, S.G., Yang, Y., Deng, B., Zhong, Y., Wen, L., Sun, W., Li, Z.W., Jansa, L., Li, J.X., Song, J.M., Zhang, X.H., Peng, H.L., 2021. Tectonic evolution of the Sichuan Basin, Southwest China. Earth Sci. Rev. 213, 103470. https://doi.org/10.1016/j.earscirev.2020.103470.
- Lloyd, M.K., Ryb, U., Eiler, J.M., 2018. Experimental calibration of clumped isotope reordering in dolomite. Geochem. Cosmochim. Acta 242, 1–20. https://doi.org/ 10.1016/j.gca.2018.08.036.
- Ma, Y.S., Zhang, S.C., Guo, T.L., Zhu, G.Y., Cai, X.Y., Li, M.W., 2008. Petroleum geology of the Puguang sour gas field in the Sichuan Basin, SW China. Mar. Petrol. Geol. 25, 357–370. https://doi.org/10.1016/j.marpetgeo.2008.01.010.
- Magara, K., 1976. Thickness of removed sediments, paleopore pressure, and paleotemperature, southwestern part of Western Canada Basin. AAPG (Am. Assoc. Pet. Geol.) Bull. 60, 554–565.
- Passey, B.H., Henkes, G.A., 2012. Carbonate clumped isotope bond reordering and geospeedometry. Earth Planet Sci. Lett. 351, 223–236. https://doi.org/10.1016/j.epsl.2012.07.021
- Rosales, I., Quesada, S., Robles, S., 2004. Paleotemperature variations of Early Jurassic seawater recorded in geochemical trends of belemnites from the Basque-Cantabrian Basin, Northern Spain. Palaeogeogr. Palaeoclimatol. Palaeoecol. 203, 253–275. https://doi.org/10.1016/S0031-0182(03)00686-2.
- Ryb, U., Eiler, J.M., 2018. Oxygen isotope composition of the Phanerozoic ocean and a possible solution to the dolomite problem. Proceeding of the National Academy of Sciences of the United States of America 115, 6602–6607. https://doi.org/10.1073/pnas.1719681115.
- Ryb, U., Lloyd, M.K., Eiler, J.M., 2021. Carbonate clumped isotope constraints on burial, uplift and exhumation histories of the Colorado Plateau. Earth Planet Sci. Lett. 566, 116964. https://doi.org/10.1016/j.epsl.2021.116964.
- Stolper, D.A., Eiler, J.M., 2015. The kinetics of solid-state isotope-exchange reactions for clumped isotopes: A study of inorganic calcites and apatites from natural and experimental samples. Am. J. Sci. 315, 363–411. https://doi.org/10.2475/05.2015.01.

Suan, G., Mattioli, E., Pittet, B., Lécuyer, C., Suchéras-Marx, B., Duarte, L.V., Philippe, M., Reggiani, L., Martineau, F., 2010. Secular environmental precursors to Early Toarcian (Jurassic) extreme climate changes. Earth Planet Sci. Lett. 290, 448–458. https://doi.org/10.1016/j.epsl.2009.12.047.

- Sweeney, J.J., Burnham, A.K., 1990. Evaluation of a simple model of vitrinite reflectance based on chemical kinetics. AAPG (Am. Assoc. Pet. Geol.) Bull. 74, 1559–1570. https://doi.org/10.1306/0C9B251F-1710-11D7-8645000102C1865D.
- Veizer, J., Prokoph, A., 2015. Temperatures and oxygen isotopic composition of Phanerozoic oceans. Earth Sci. Rev. 146, 92–104. https://doi.org/10.1016/j. earscirev.2015.03.008.
- Veizer, J., Bruckschen, P., Pawellek, F., Diener, A., Podlaha, O.G., Carden, G.A.F., Jasper, T., Korte, C., Strauss, H., Azmy, K., Ala, D., 1997. Oxygen isotope evolution of Phanerozoic seawater. Palaeogeogr. Palaeoclimatol. Palaeoecol. 132, 159–172. https://doi.org/10.1016/S0031-0182(97)00052-7.
- Veizer, J., Ala, D., Azmy, K., Bruckschen, P., Buhl, D., Bruhn, F., Carden, G.A.F., Diener, A., Ebneth, S., Godderis, Y., Jasper, T., Korte, C., Pawellek, F., Podlaha, O. G., Strauss, H., 1999. ⁸⁷Sr/⁸⁶Sr, 8¹³C and 8¹⁸O evolution of Phanerozoic seawater. Chem. Geol. 161, 59–88. https://doi.org/10.1016/S0009-2541(99)00081-9.
- Wallmann, K., 2001. The geological water cycle and the evolution of marine $\delta^{18}O$ values. Geochem. Cosmochim. Acta 65, 2469–2485. https://doi.org/10.1016/S0016-7037(01)00603-2.
- Wang, X., Cui, L., Li, Y., Huang, X., Zhai, J., Ding, Z., 2016a. Determination of clumped isotopes in carbonate using isotope ratio mass spectrometry: Toward a systematic evaluation of a sample extraction method using a static PorapakTM Q absorbent trap. Int. J. Mass Spectrom. 403, 8–14. https://doi.org/10.1016/j.ijms.2016.03.008.
- Wang, X., Cui, L., Zhai, J., Ding, Z., 2016b. Stable and clumped isotopes in shell carbonates of land snails *Cathaica* sp. and *Bradybaena* sp. in North China and implications for ecophysiological characteristics and paleoclimate studies. Geochem. Geophys. Geosystems 17, 219–231. https://doi.org/10.1002/ 2015GC006182.
- Wang, X., Jin, Z., Zhao, J., Zhu, Y., Hu, Z., Liu, G., Jiang, T., Wang, H., Li, S., Shi, S., 2020. Depositional environment and organic matter accumulation of Lower Jurassic nonmarine fine-grained deposits in the Yuanba Area, Sichuan Basin, SW China. Mar. Petrol. Geol. 116, 104352. https://doi.org/10.1016/j.marpetgeo. 2020.104352.

- Wang, Z., Li, X., Deng, Y., Zhang, Y.Y., Liu, X., 2023a. Stable isotope evidence confirms lakes are more sensitive than rivers to extreme drought on the Qinghai-Tibet Plateau, China. J. Hydrol. 627, 130446. https://doi.org/10.1016/j.ihydrol.2023.130466.
- Wang, X., Dong, L., Li, T., Wang, Z., Zhang, C., Jin, Z., Fu, J., Zhu, R., Ling, K., Wang, T., 2023b. Late diagenetic alteration of carbonate evidenced by carbonatedeficient siliciclastic laminae. Chem. Geol. 622, 121394. https://doi.org/ 10.1016/j.chemgeo.2023.121394.
- Winkelstern, I.Z., Lohmann, K.C., 2016. Shallow burial alteration of dolomite and limestone clumped isotope geochemistry. Geology 44, 467–470. https://doi.org/10.1130/G37809.1.
- Wu, Y., Wu, Z., 1996. Two-phase diagenetic alteration of carbonate matrix: Middle Ordovician limestones, Taiyuan City area, China. Sediment. Geol. 106, 177–191. https://doi.org/10.1016/0037-0738(95)00156-5.
- Xu, Q., Liu, B., Ma, Y., Song, X., Wang, Y., Chen, Z., 2017a. Geological and geochemical characterization of lacustrine shale: a case study of the Jurassic Da'anzhai member shale in the central Sichuan Basin, Southwest China. J. Nat. Gas Sci. Eng. 47, 124–139. https://doi.org/10.1016/j.jngse.2017.09.008.
- Xu, W., Ruhl, M., Jenkyns, H.C., Hesselbo, S.P., Riding, J.B., Selby, D., Naafs, B.D.A., Weijers, J.W.H., Pancost, R.D., Tegelaar, E.W., Idiz, E.F., 2017b. Carbon sequestration in an expanded lake system during the Toarcian oceanic anoxic event. Nat. Geosci. 10, 129–134. https://doi.org/10.1038/NGE02871.
- Xu, Q., Hao, F., Ma, Y., Liu, B., Song, X., 2020. Effects of the matrix on the oil production of super tight limestone in a lacustrine mixed sedimentary environment: the case of the Jurassic Da'anzhai member in the central Sichuan Basin, China. Mar. Petrol. Geol. 121, 104583. https://doi.org/10.1016/j.marpetgeo.2020.104583.
- Zhai, G.M., 1989. Petroleum Geology of China, vol. 10. Petroleum Industry Press, Beijing (in Chinese).
- Zhu, R., Zhao, X., Liu, L., Wang, X., Zhang, N., Guo, H., Song, L., 2009. Depositional system and favorable reservoir distribution of Xujiahe Formation in Sichuan Basin. Petrol. Explor. Dev. 36, 46–55. https://doi.org/10.1016/S1876-3804(09) 60110-5.
- Zhu, C.Q., Hu, S.B., Qiu, N.S., Rao, S., Yuan, Y.S., 2016. Thermal history of the Sichuan Basin, SW China: Evidence from deep boreholes. Sci. China Earth Sci. 59, 70–82. https://doi.org/10.1007/s11430-015-5116-4.